Electronic Supplementary Material (ESI) for Soft Matter.

Barrier kinetics of adsorption-desorption of alcohol monolayers on water under constant surface tension

(supplementary information)

Ivan L. Minkov,[a,b] Dimitrinka Arabadzhieva,[c] Ibrahim E. Salama,[d,e]
Elena Mileva,[c] Radomir I. Slavchov*[,f,g]

[a] *Department of Physical Chemistry, Faculty of Chemistry and Pharmacy, Sofia University, 1 J. Bourchier Blvd., 1164 Sofia, Bulgaria*
[b] *Department of Chemistry, Biochemistry, Physiology, and Pathophysiology, Faculty of Medicine, Sofia University, 1 Koziak Str., 1407 Sofia, Bulgaria*
[c] *Bulgarian Academy of Science, Akad. G. Bonchev Str., bl.11, 1113 Sofia, Bulgaria, Sofia, Bulgaria*
[d] *Department of Chemisty, Cambridge University, CB2 1EW Cambridge, United Kingdom*
[e] *BP Institute, Cambridge University, Bullard Laboratories, Madingley Road, CB3 0EZ Cambridge, United Kingdom*
[f] *Department of Chemical Engineering and Biotechnology, Cambridge University, Philippa Fawcett Drive, West Site, CB3 0AS Cambridge, United Kingdom*
[g] *School of Engineering and Materials Science, Queen Mary University of London, Mile End Road, London E1 4NS, United Kingdom*
**E-mail: ris26@cam.ac.uk*

S1. List of symbols

A	area covered by the monolayer
A_0	area covered by the monolayer in the initial moment
C	concentration of the surfactant
$C(z = 0)$	subsurface surfactant concentration (right next to the surface)
C_{eq}	equilibrium surfactant concentration with respect to monolayer, $C_{eq} = \gamma^S \Gamma / K_a$
C_s	solubility of surfactant crystals
D	diffusion coefficient of the surfactant
j^S	rate of the (monolayer)→(subsurface) barrier process of desorption, $j^S = v_d - v_a$
K^{LC}	the empirical coefficient in eqn (24) for τ_d vs. Γ^{-1} in the LC phase
K^{LE}	the empirical coefficient in eqn (24) for τ_d vs. Γ^{-1} in the LE phase
K_a	adsorption constant of the surfactant
k_B	Boltzmann constant
k_d	rate constant for desorption, $v_d = k_d C_{eq}$
k_Γ	rate constant for desorption of Motomura et al., $v_d = k_\Gamma \Gamma$
n	amount of surfactant in the monolayer [mol]

T	temperature
t	time
t_{max}	experimental time for transition to convective diffusion regime
v_a	adsorption rate, $v_a = k_d C(z = 0)$
v_d	desorption rate, $v_d = k_d C_{eq}$
z	cartesian coordinate normal to the surface
α	hard disc area of an adsorbed surfactant molecule ($\alpha = 16.5$ Å^2 for alcohols)
$\alpha_\perp$	crystallographic/collapse area, $\alpha_\perp = 1.1\alpha = 18.2$ Å^2 for alcohols
β	lateral attraction parameter
Γ	adsorption of the surfactant
γ^S	surface activity coefficient of the surfactant
μ	chemical potential of the surfactant monolayer
μ_0	standard chemical potential
μ_s	chemical potential of the surfactant crystal
$\Delta_s\mu$	$= \mu - \mu_s$
π^S	surface pressure, $\pi^S = \sigma_0 - \sigma$
σ	surface tension
σ_0	surface tension of the neat surface of the solution
σ_s	the value of σ for the crystal's spread monolayer

$\tau_d = \Gamma/k_d C_{eq}$, characteristic time for desorption

$\tau_{tr} = D/k_d^2$, characteristic time for transition from barrier to diffusion controlled regime

S2. The Wilhelmy method and the surface tension of water

To determine the surface tension, we measured the weight of a 19.53 mm wide platinum plate attached at the studied surface. As all techniques for surface tension measurement, the combined Langmuir trough/Wilhelmy plate method is not straightforward to use and requires special measures to be taken against artefacts. The main problems associated with it are

(i) fouling with surface active impurities has to be avoided;

(ii) complete wetting of the plate is required;

(iii) the location of the plate with respect to the surface has to be fixed (slow evaporation can lead to a decrease of the water level, and fast barrier movement can increase the water level, affecting the results);

(iv) a number of dynamic effects (kinetics of adsorption and desorption; natural convection and convection due to the movement of the barrier; leakage of surfactant through the barrier; evaporation of the water, the surfactant, and the organic solvent in which the surfactant is

dissolved upon spreading; deboarding, collapse and slow kinetics of phase transitions in the monolayer) have to be considered when the data is interpreted;

(v) in the case where the spreading pressure of crystals is measured, crystals often attach to the plate and alter the signal.

Details on the procedures that we use against these artefacts as a standard in our laboratory are given in ref. [17] (surface rinsing, cleaning and prewetting of the plate *etc.*). With regard to (i) and (ii), pure water is the worst-case scenario: in the presence of a dense monolayer of the studied surfactant, impurities affect little the state of the surface, and the wetting is significantly improved. Therefore, we measured the surface tension σ_0 of pure water before each experiment. The measured σ_0 are shown in Figure S1 as a function of T. The line is a linear regression over the data, and gives σ_0/[mN/m] = 75.64-0.138T(°C), in excellent agreement with the accepted literature values. However, the standard deviation is significant: 0.3 mN/m.

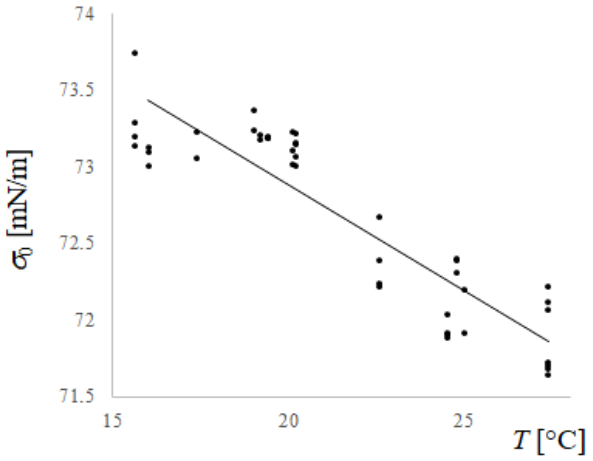

Figure S1. Surface tension of water.

S3. Measuring the spreading tension with bubble profile analysis in saturated aqueous dodecanol

For the measurements with bubble profile analysis tensiometer we used the same saturated dodecanol solutions as for experiments with the Langmuir trough. The work area of the apparatus is set to the required temperature by a thermostat. A quartz crystal cuvette is filled with 25 mL solution, saturated at the desired temperature. The cuvette is then covered with a top through which a glass capillary is fitted and dipped into the solution. An air bubble with a fixed area is formed at the tip of the capillary end and then the experiment is started. The apparatus is recording the surface tension variation with time, caused by dodecanol adsorption. During the experiment the surface area of the bubble is kept constant. The duration of the experiments was 4-6 hours, and continued until the surface tension vs. t curve reaches a plateau value.

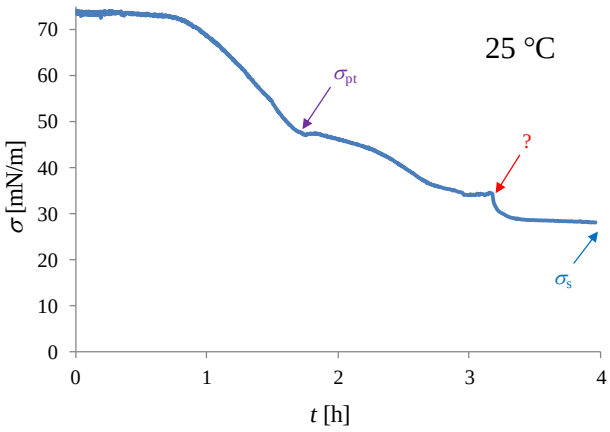

Figure S2. Dynamic surface tension of a bubble in saturated $C_{12}H_{25}OH$ solution at 25 °C.

The first kink in Figure S2 (the small plateau portion indicated with σ_{pt}) corresponds to the LE-LC phase transition. We are unsure what could be the reason the second kink (marked with "?") – we observed the same feature at 17 °C. No similar feature is observed at this particular surface tension in the σ vs. $1/\Gamma$ isotherm, see Figure 2. The shape of it suggests a sudden increase in the rate of the adsorption, which might correspond to a convection transition similar to those occurring in the isobaric desorption experiments (the arrow in Figure 6). The curve reaches a plateau after 4 h, corresponding to saturation of the surface and to value of σ equal to the spreading tension of crystals (σ_s in the Figure S2).

S4. Correcting the adsorption isotherms for the solubility of the dodecanol and the kinetics of the LE-LC phase transition

We compressed the monolayer as quickly as possible to minimize the losses due to dissolution (a compression run takes less than a minute). This option has a price – the monolayer needs some time to relax to its equilibrium state, especially in the region where the phase transitions gas-LE and LE-LC occur. If the compression is fast enough, we can approximately assume that the desorption is under barrier control. In this case, the flux of surfactant out of the surface is given by $j^S = k_d C_{eq} = \Gamma/\tau_d$ and the mass balance of the surface is given by the equation

$$\frac{1}{A}\frac{\mathrm{d}n}{\mathrm{d}t} = -\frac{\Gamma}{\tau_d}, \qquad (1)$$

compare to eqn (12). This equation is valid for both the isobaric runs and the normal compressions. For the isobaric regime of the Langmuir balance, where the adsorption Γ is constant, eqn (1) leads to

$$\frac{1}{A}\frac{\mathrm{d}A}{\mathrm{d}t} = -\frac{1}{\tau_d}, \quad \text{and} \quad \ln\frac{A}{A_0} = -\frac{t}{\tau_d}, \qquad (2)$$

i.e. eqn (14).

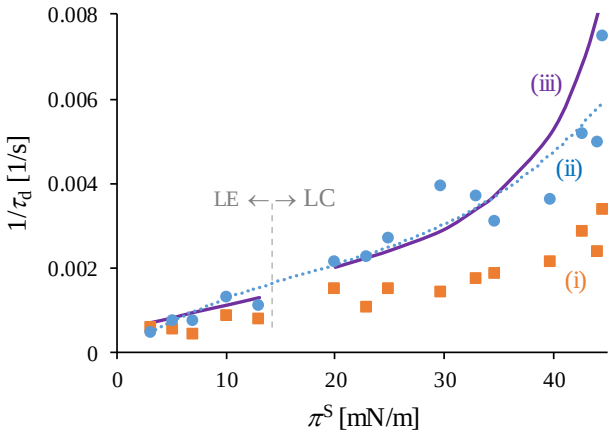

Figure S3. Reciprocal desorption time $1/\tau_d$ as a function of the surface pressure: results from isobaric desorption experiments at 17 °C. Orange squares: 1st iteration (2-parametric fits with eqn (13)). Blue circles: 2nd iteration (1-parametric fits with eqn (13)). Blue dot line: polynomial regression with eqn (3). Solid line: last iteration, eqn (24)&(16).

For every temperature and every surface pressure value, we fitted the isobaric data with eqn (13), as a first iteration, in order to determine both τ_d and τ_{tr}. The results are not very accurate, but still good enough for the correction. The data for $1/\tau_d$ as function of π^S are given in Figure S3 (orange squares). The results were interpolated using the regression formula:

$$\frac{1}{\tau_d} = c_1\pi^S + c_2\left(\pi^S\right)^2 + c_3\left(\pi^S\right)^3 \ldots \qquad (3)$$

We found that a quadratic or cubic polynomial is sufficient for the regression. The desorption time τ_d is assumed to tend to infinity when $\pi^S = 0$ (infinitely dilute monolayer); therefore, eqn (3) has no constant term.

With τ_d known, we can proceed to the integration of the kinetic equation (1) for the normal compression run to obtain the dependence of the total adsorbed quantity on time, $n(t)$. We multiply both sides of eqn (1) by $\Gamma^{-1}\mathrm{d}t$, and use that $n/A = \Gamma$:

$$\frac{\mathrm{d}n}{n} = -\frac{\mathrm{d}t}{\tau_d}. \qquad (4)$$

Integration yields:

$$\ln\frac{n}{n_0} = -J, \qquad \text{where } J = \int_0^t \tau_d^{-1}\mathrm{d}t. \qquad (5)$$

The integral J can be computed at each time step of the compression run using the following recurrent formulation of the Newton trapezium method:

$$J_1 = t_1\tau_{d,1}^{-1}/2; \quad J_{i+1} = J_i + \left(t_{i+1} - t_i\right)\left(\tau_{d,i+1}^{-1} + \tau_{d,i}^{-1}\right)/2; \qquad (6)$$

here, $\tau_{d,i} = \tau_d(\pi_i^S)$, as given by the interpolation (3), and π_i^S is the surface pressure measured at time t_i. Once J_i is known, we use eqn (5) in the form

$$\Gamma = \frac{n}{n_0}\Gamma_{app} = \Gamma_{app}\exp(-J). \qquad (7)$$

In all cases, we did one or two iterations by using the results from Sec. 3.4 for τ_d, *i.e.*

(i) we used the first iteration for Γ from eqn (7) to compute the solubility of the monolayer used in Sec. 3.4 to deal with the isobaric data and calculate the second iteration for τ_d (the first being the one obtained from the 2-parameter fit, orange squares in Figure S3, and the second being the blue circles).

(ii) We used the second iteration for τ_d to compute a new interpolation according to eqn (3), and use this interpolation in eqn (5) to produce a second iteration for J.

(iii) The new J has been used to produce a second iteration for Γ via eqn (7).

The improvement from the iterations after the first was insignificant, even though the difference between the τ_d in Figure S3 and the more accurate ones obtained in Sec. 3.4 is often large in the LC region.

Our previous procedure for solubility correction has been tested in ref. [17] by comparing the results from monolayer compression at different rates of motion of the barrier of the trough. We did a similar test with the new procedure. Two compression runs of dodecanol monolayer at 25 °C were performed, one at the highest possible velocity of the barrier, 270 mm/min, and the other at a 3-fold lower speed of 90 mm/min. The results before and after the correction are illustrated in Figure S4. Before the correction, the slow isotherm is visibly shifted towards lower areas. After the correction, the two are in reasonable agreement, which proves the usefulness of the procedure. For the higher velocity, the correction leads to actual areas per molecule by 1-2 Å^2 larger than the apparent areas (and less for lower temperatures). The figure also gives an idea of how bad the assumption for desorption under barrier control is: the slight misfit of the two curves is because of the overcorrection of the slower isotherm (where diffusion slows down the process additionally, which is not accounted for in the correction procedure). As seen, the difference is small enough to ignore (smaller than the reproducibility of the isotherms).

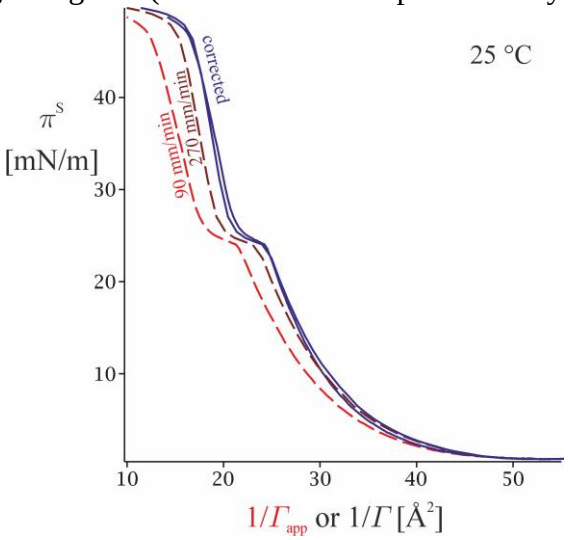

Figure S4. Surface tension vs. apparent area and corrected area per molecule of dodecanol spread on water at 25 °C: data for two barrier velocities, 90 and 270 mm/min. The dashed lines are before the correction.

Our dodecanol isotherms can be compared with those of Fainerman et al. [50] at 10 and 15 °C. Especially at 15 °C, their results are shifted towards higher densities (Figure S5); the LC region is approaching unrealistic areas smaller than the crystallographic area of solid alkanes ($1/\Gamma < 18.2$ Å^2). This means that the data from [50] are significantly affected by solubility as well. In addition, the LE-LC phase transition of Fainerman et al. is at slightly higher surface pressure than ours. This can be explained either by the presence of impurities in theirs or our dodecanol, or by imperfect thermostating (the temperatures of Fainerman et al. appear to have been by ~2° higher than ours).

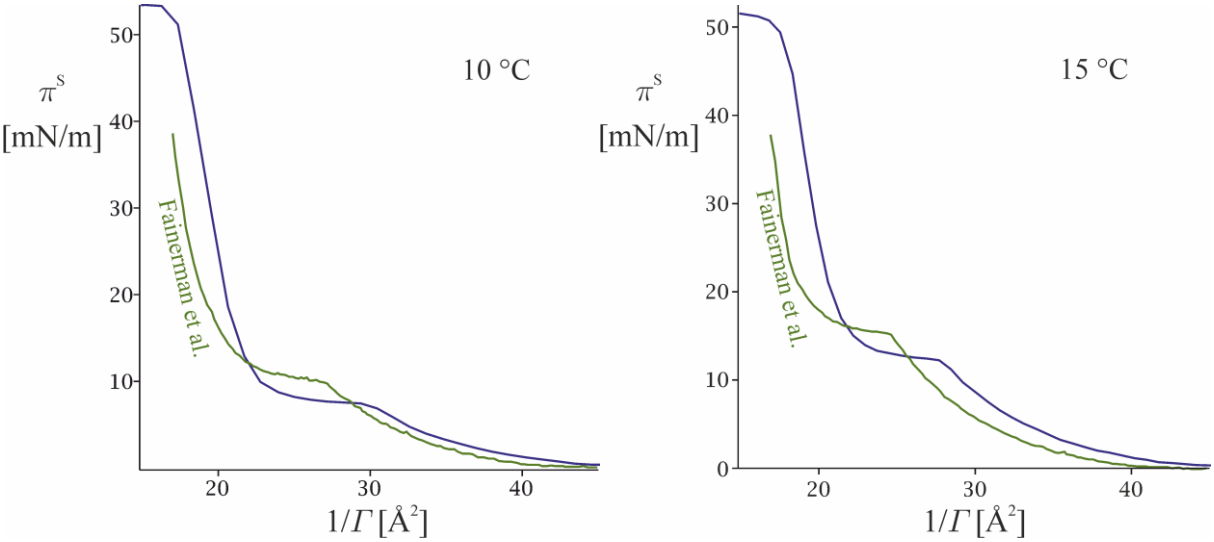

Figure S5. Comparison between our isotherms at 10 and 15 °C and those by Fainerman et al. [50].

Kinetics of the LE-LC phase transition. Since we compress the monolayer quickly, we have to correct for the increased dynamic surface pressure in the phase transition region. Once the LC domains are formed, they start to interact repulsively with each other [51], and the force applied by the barrier on the heterogeneous monolayer is partly acting against this repulsive force (similar effects are common in the three dimensional liquid-solid phase transitions, when the fractal net of solid crystals in touch with each other start to have an elastic answer against the external force). The LC region covers a very short range of areas, and we usually have only 5-6 points in this region; the first few of them are affected by the dynamics of the phase transition, and the last few are affected by the collapse. In view of these complications, we decided that the crudest approximation for the equilibrium shape of the LC region – a line – is good enough. The following procedure was applied to all data:

(i) Identify the point at which the phase transition starts (indicated with an arrow in Figure S6); the data right of this point corresponds to homogeneous LE phase, while the data left of it refers to a heterogeneous surface with LC domains dispersed in an LE film (probably, the system relaxes to homogeneous LC monolayer eventually, but it is very likely that the LC

domains and the two-dimensional LE films between them will survive even at significant compressions, close to the collapse).

(ii) The data in the LE region are fitted with eqn (16) ($\pi^S > \pi^S_{pt}$) – let the respective function be $f^{LE}(\pi^S)$. The data for the heterogeneous monolayer is fitted with a polynomial (of degree 3 or 4); we call the respective function $f^{het}(\pi^S)$.

(iii) The point at which $f^{LE}(\pi^S) = f^{het}(\pi^S)$ identifies the phase transition pressure tension π^S_{pt} and the respective equilibrium LE adsorption Γ^{LE}.

(iv) The data for the heterogeneous monolayer has an inflection. The tangent line through the inflection point of f^{het} is constructed and is assumed to represent the equilibrium state of the LC monolayer (the equilibrium LC line in Figure S6).

(v) The point of cross-section of the equilibrium LC line and the horizontal line $\pi^S = \pi^S_{pt}$ defines the area of the LC monolayer in equilibrium with the LE film.

(vi) The value of the equilibrium spreading pressure π^S_{pt} is substituted in the equation for the equilibrium LC line; this yields the area of the equilibrium spread layer.

This procedure is illustrated in detail in Figure S6, and also in Figure 2, in less detail. The edges of the horizontal dashed lines are part of the binodal for the LE-LC transition. It is remarkable that the slope of the LC region in Figure 2 (*right*) does not depend on the temperature significantly. The parameters of eqn (16) obtained via this procedure are summarized in Table .

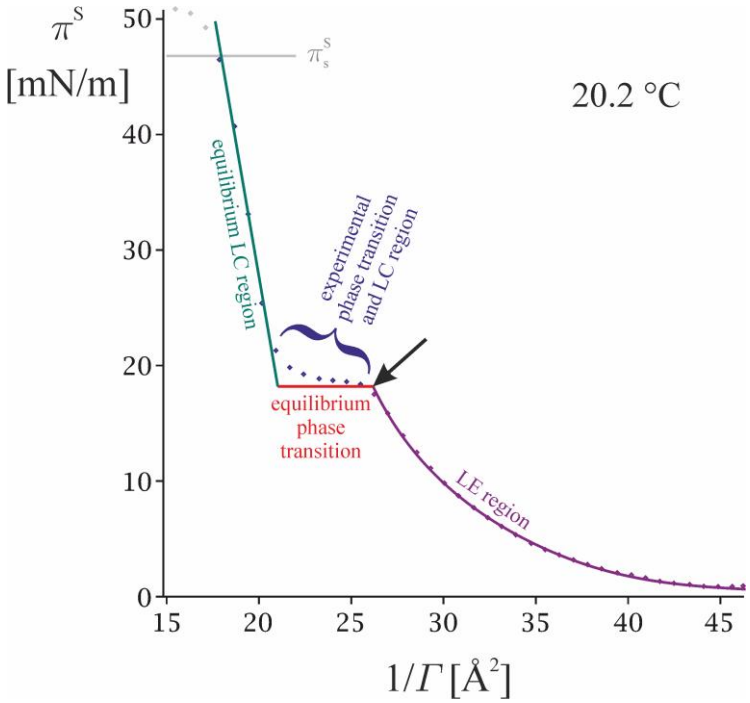

Figure S6. Correction for the kinetic effects during the LC-LE phase transition. The significant repulsion between the LC domains formed during the phase transition leads to a kinetic increase of the surface pressure π^S. The observed π^S vs. Γ^{-1} curve in this region is therefore below the theoretically expected horizontal line for a first order phase transition.

Table S1. Parameters of the equation of state (16), as obtained from the corrected π^S vs. $1/\Gamma$ isotherms.

T	10 °C	15.4 °C	17 °C	20.2 °C	22.9 °C	25 °C
g_1 [Å^2]	24.2836	30.4535	31.4014	22.2778	23.07556	14.2358
g_2	-0.0269519	-0.238060	-0.238816	-0.134695	-0.121569	-0.0585756
g_3	-0.972393	-0.758748	-0.755349	-0.859611	-0.872810	-0.934531
m_1	1	5	4	2	2	1
m_2	30	19	15	14	14	19
m_3	1	3	2	2	2	2
g_4 [Å^2]	22.5770	22.2171	22.1276	22.9717	23.6772	24.8072
g_5 [Å^{2}m/mN]	0.0978461	0.0875110	0.0762142	0.107170	0.105664	0.146501
π^S_{pt} [mN/m]	7.38686	12.1554	14.5308	18.1982	20.8908	23.8605
a^{LE}_{pt} [Å^2]	30.07	28.2120	27.0654	26.1812	26.0406	25.0290
a^{LC}_{pt} [Å^2]	21.85	21.1534	21.0201	21.0214	21.4697	21.3116
$a_{collapse}$ [Å^2]	18.00	18.12	18.56	17.96	18.73	17.9492

Figure S7 illustrates the computation via the Gibbs equation (3) of the chemical potential $\Delta_s\mu = \mu - \mu_s$ from the isotherm fits just discussed. The state of the surfactant in the crystal is used as a standard state – the integration starts at the spreading pressure of dodecanol crystals.

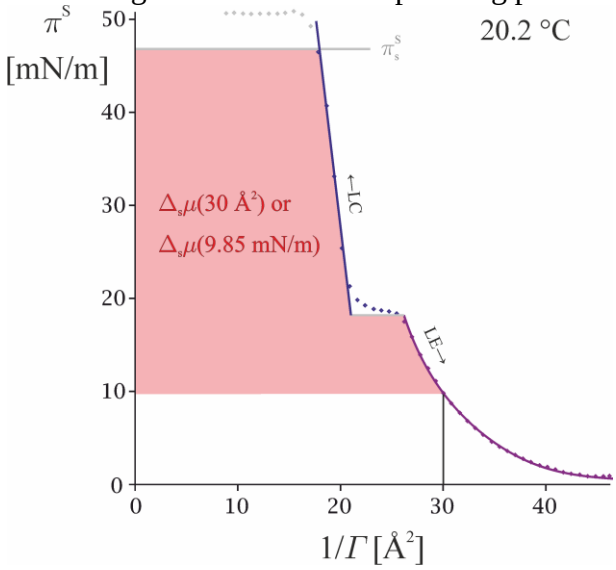

Figure S7. Graphical representation of the chemical potential $\Delta_s\mu$. The surface pressure vs. area isotherm at 20.2 °C is used to compute the value of $\Delta_s\mu$ at π^S = 9.85 mN/m (corresponding to $1/\Gamma$ = 30 Å^2). According to eqn (3), $\Delta_s\mu$ is given by minus the shaded area. π^S_s is the spreading pressure of dodecanol crystals.

For the sake of completeness and for future reference, we also analysed the data for the LE-LC phase transition pressure π_{pt}^{S} as a function of temperature. Unlike the area per molecule, the surface pressure of the phase transition is unaffected by the desorption and the leakages, so we collected a significant amount of data in the range 10-30 °C, Figure S8. The line in this figure is a quadratic fit. Using the data for π_{pt}^{S} from Figure S8 and the phase transition areas a_{pt}^{LE} and a_{pt}^{LC} from Table , we were able to compute the heat of the phase transition Δh_{pt} through the 2D-Clausius-Clapeyron equation,

$$\frac{d\pi_{pt}^{S}}{dT} = \frac{\Delta h_{pt}}{T\left(a_{pt}^{LE} - a_{pt}^{LC}\right)}. \qquad (8)$$

The dependence of Δh_{pt} on T that follows from this equation is illustrated in Figure S9.

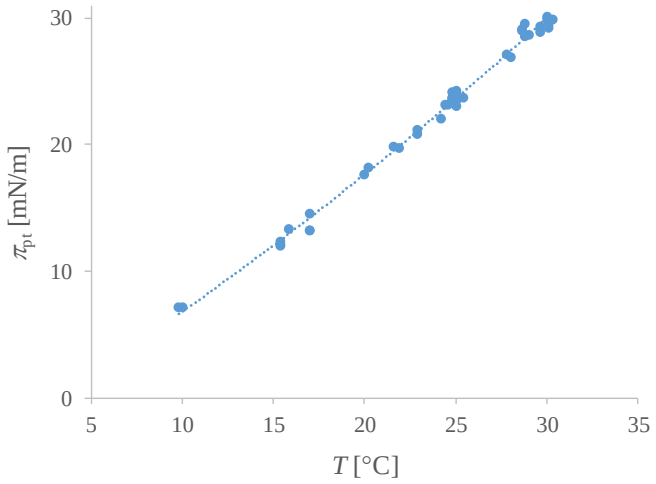

Figure S8. Surface pressure of the LE-LC phase transition as a function of the temperature.

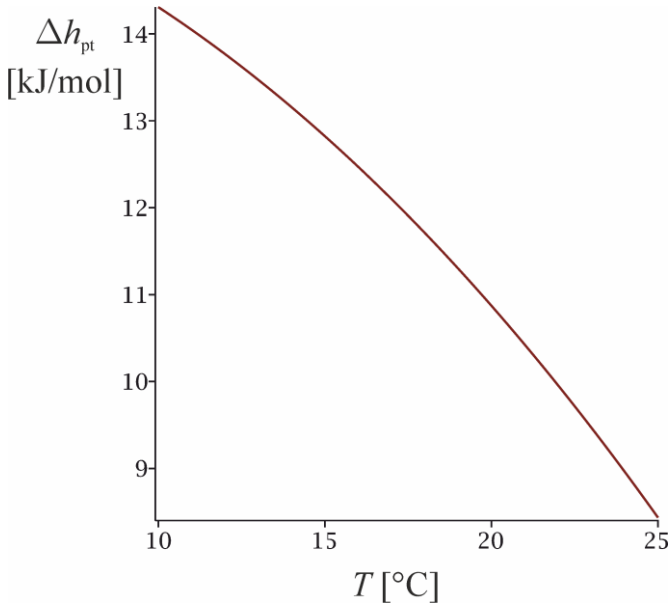

Figure S9. Heat of the LE-LC phase transition.

S5. Leakage through the barrier

The test involved placement of dodecanol crystals in one compartment of the trough and measurement of the surface tension in the other (which should remain clean in the absence of leakage, $\sigma = \sigma_0$), with a barrier separating the two compartments. In the first run (the upper curve in Figure S10), leakage was negligible for 4 minutes, then it caused the observed decrease of σ in the crystal-free compartment. In the second run (lower curve), leakage was immediately apparent. The plateau reached at the 3rd minute corresponds to the LE-LC phase transition.

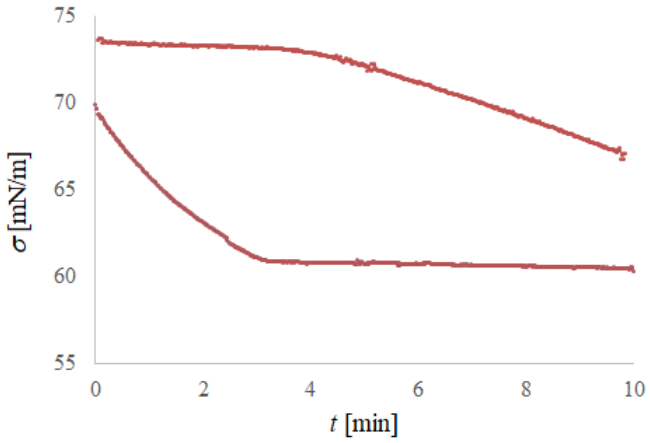

Figure S10. An illustration of random leakage through the movable barrier: in both runs, crystallites are placed in one of the compartments to form an equilibrium spread monolayer at 16 °C. The surface tension in the second compartment (the surface of which is initially alcohol-free) is measured as a function of time.

S6. Dodecanol – additional data

Here, we present most of our desorption isobars at temperatures from 10 to 23 °C (Figure S11, points). These are compared to the theoretical model (13), with value of τ_d from eqn (24)-(25) and value of τ_{tr} from eqn (11), with the parameters from Table 2.

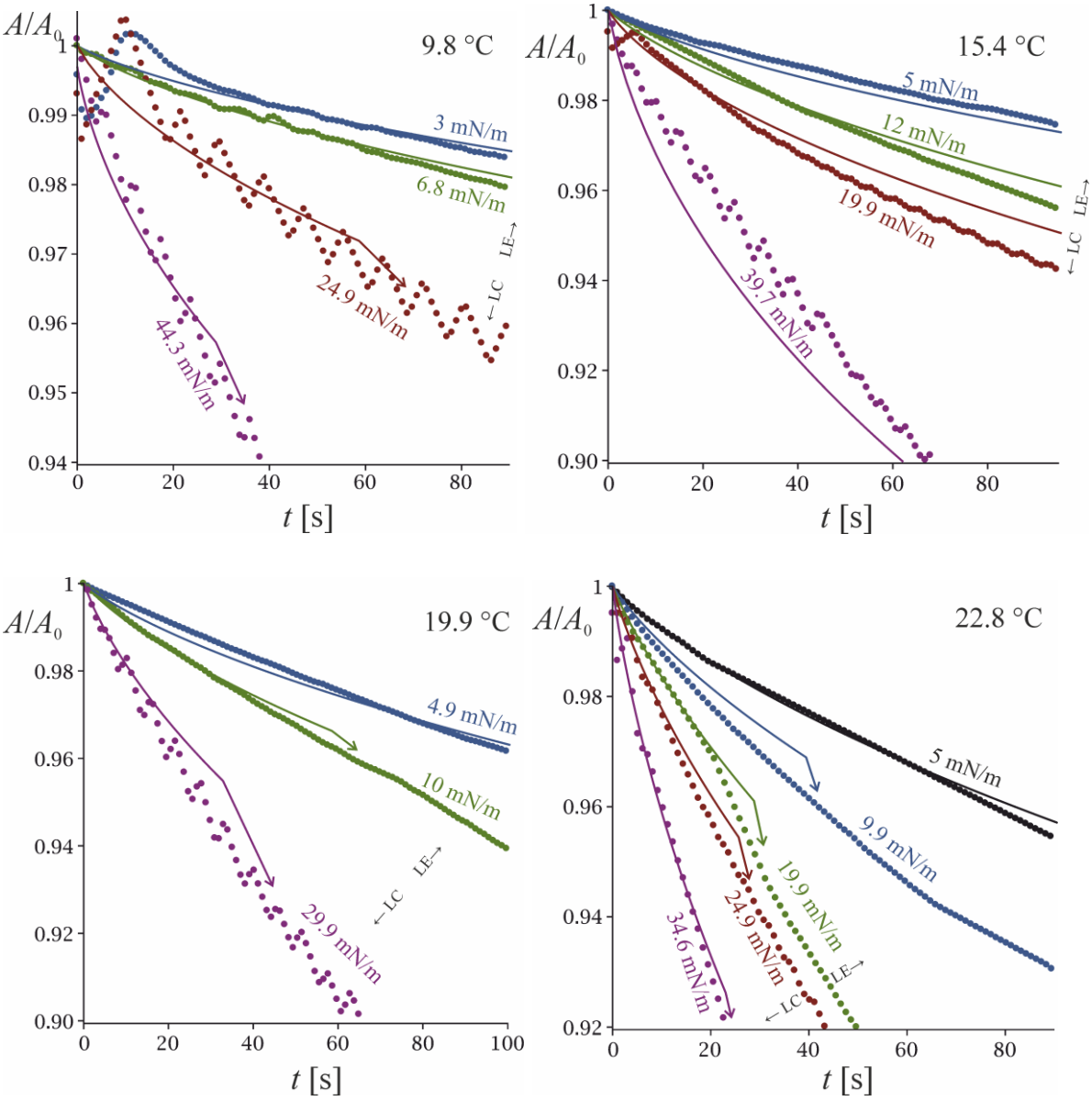

Figure S11. Desorption isobars (relative decrement of the area vs. time) at several fixed surface pressures and temperatures. Solid lines: the theoretical prediction (13) for mixed barrier-diffusion control, with desorption time τ_d linear with $1/\Gamma$ (eqn (24) with K^{LE} and K^{LC} from Table 2).

At higher temperatures (25—30 °C), the desorption is under barrier control as in Figure 9. However, due to the leakages, we were unable to measure the adsorption isotherms at 29 and 30 °C, although we measured desorption isobars. Therefore, in Figure S12, the measured isobars are presented without comparison to theory. We attempted to estimate the required quantities (τ_d and Γ) by extrapolation of the π^S vs. $1/\Gamma$ isotherms in Figure 2 and the τ_d formulae (24)-(25) (which are strictly valid in the range 10-25 °C). Overall, the observed desorption rates seem to be slightly faster than the predicted ones from this extrapolation (as if the real τ_d at 30 °C is by *ca.* 25% smaller than the extrapolated). This might mean that the activation energy E_A^{LE} is underestimated, but might also be due to leakages, evaporation or, in part, to inaccurate extrapolation of the compression isotherm.

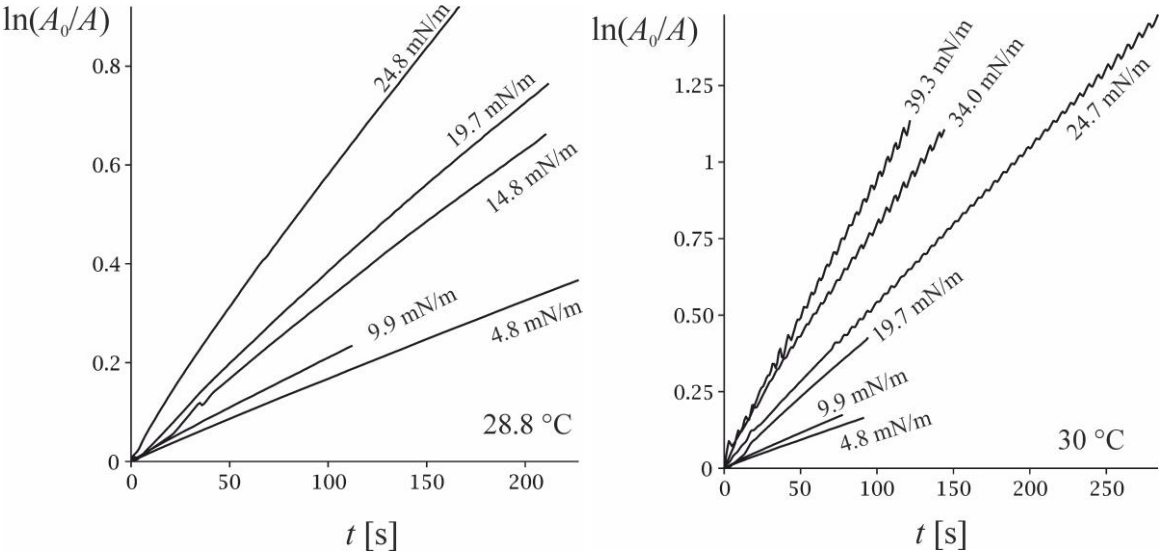

Figure S12. Desorption isobars at 29-30 °C and several fixed surface pressures. The process seems to proceed under barrier control (similarly to the data at 25 °C in Figure 9) for at least 50-100 s, but in the absence of compression isotherm data, we did not try to interpret these data.

In Figure 13, the data of De Keyser and Joos for dodecanol is compared with the theoretical prediction for desorption under pure barrier control (dashed line) and desorption in the τ_d-D regime (solid line). As discussed in sec. 4, in the time range of interest to us (0-200 s), the data indeed suggests barrier control, exactly as our measurements at 25 °C (Figure 9).

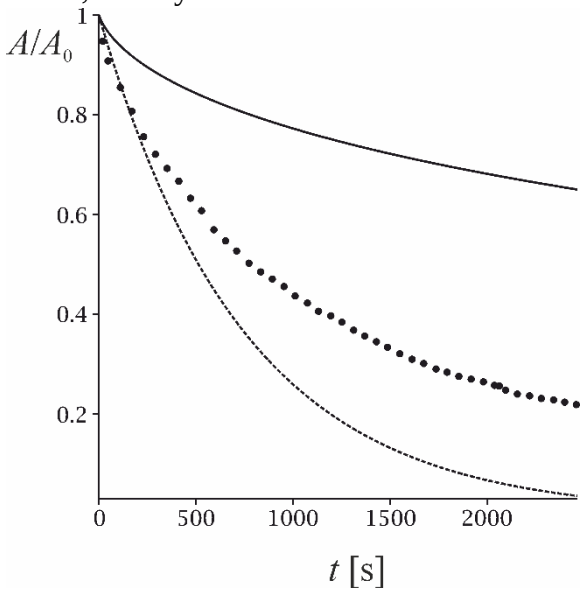

Figure 13. Desorption isobar by De Keyser and Joos at 8 mN/m (probably 25 °C). Solid line: the theoretical prediction (13) for mixed barrier-diffusion control. Dashed line: pure barrier control, eqn (14). The adsorption Γ and the desorption time τ_d at 8 mN/m were calculated from eqn (16)&(24).

Figure S14 illustrates the dispersion analysis of the fit of the τ_d data in Table 2 with eqn (24)-(25). All values of the parameters K_0 and E_A that fall inside the ellipses "1.05 × dev^2_{min}" will produce dispersion by 5% larger than the minimal.

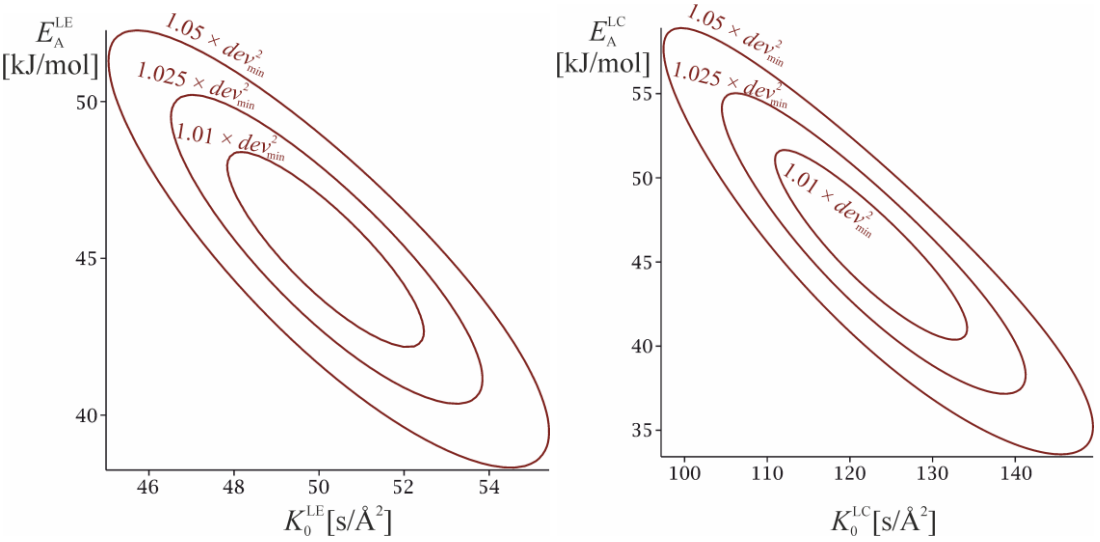

Figure S14. Contour plot of the dispersion of eqn (24)-(25) against the τ_d data in Table 2.

S7. Decanol data

The sticky disc adsorption model predicts a theoretical surface pressure vs. concentration isotherm $\pi^S_{th}(C_{eq}; K_a, \alpha, \beta)$ (a numerical solution to eqn (18)-(19)&(4)). The value of the hard-disc area α is set to the one following from crystallographic data, 16.5 Å^2. The other two parameters are obtained through minimization of the merit function

$$dev^2_\pi(K_a, \beta) = \frac{1}{N-2}\sum_i \left[\pi^S_{th}(C_i; K_a, \beta) - \pi^S_i\right]^2 . \qquad (9)$$

Here, C_i and π^S_i are the experimental surfactant concentrations and surface pressures from ref. [29,38,39,63,82]. We used only low pressure data with π^S < 30 mN/m, since it is likely that at higher surface pressures the monolayer is in the LC state where eqn (18) is invalid, and anyway, the data of Baret et al. are in the range 5—20 mN/m. The result of the regression for the best fit parameters is β = 20.7 and K_a = 39.25 μm, *i.e.* ln(K_a/[m]) = –10.15. These can be compared to β = 14 and ln(K_a/[m]) = –9.8 from ref. [60] (the latter values are not accurate enough for long-chained alcohols such as decanol). The comparison between the data points and the theoretical sticky disc curve with the best fit parameters is shown in Figure S15.

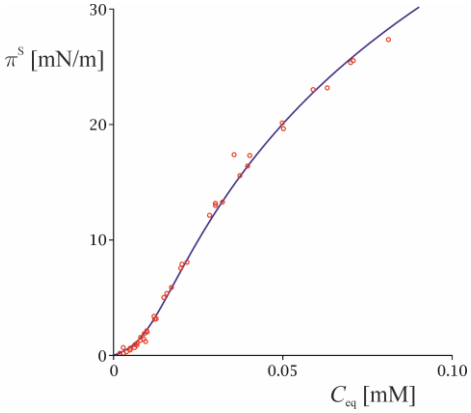

Figure S15. Adsorption isotherm of decanol: data from ref. [29,38,39,63,82] and the best fit with the sticky disc model (18)-(19)&(4), with K_a = 39.25 μm and β = 20.7.

The values obtained for K_a and β allow the computation of Γ and γ^S at each surface pressure of Baret et al. We calculated the adsorptions by solving eqn (18) for Γ; this value of Γ was further substituted in eqn (19) to find the respective surface activity coefficient γ^S. Eqn (4) was then used to calculate C_{eq}. The results for Γ and C_{eq} at the four surface pressures of Baret at al. are given in Table 3 in the main text.

This leaves a single unknown parameter in eqn (13) for the kinetics of desorption: the desorption rate constant τ_d. To find τ_d, eqn (13) has been used to fit the A vs. t data of Baret et al. [6] at each surface pressure. The results are illustrated in Figure S16, and the values of τ_d are summarized in Table 3. An acceleration of the diffusion process is evident at the longest times ($t > t_{max}$) for π^S = 5, 10 and 15 mN/m (discussed also by Baret et al. [6]) – therefore, only the data at $t < t_{max}$ were used for the regression. The times t_{max} where first signs of convective regime are seen were determined iteratively using positive deviations from eqn (13) as a criterion, similarly to the procedure for dodecanol in sec. 3.4. The time of transition is marked with red dots in Figure S16.

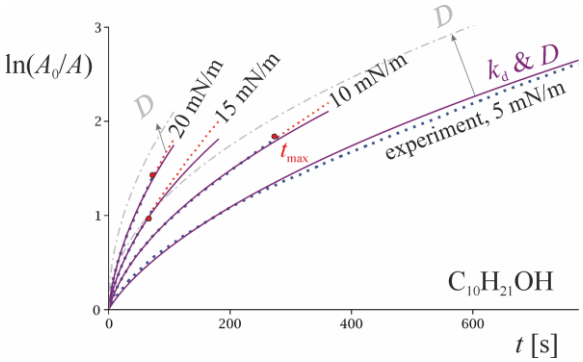

Figure S16. $\ln(A_0/A)$ vs t [s] for $C_{10}H_{21}OH$ – data from ref. [6] (dot lines) at 4 surface pressures (5-20 mN/m). Dash-dot lines: *D*-regime, eqn (15), overpredicting the dissolution rate compared to the experiment. Solid lines: fits to the experimental data of eqn (13) for the mixed barrier-diffusion mechanism (τ_d & D). The best-fit values of τ_d are listed in Table 3. Acceleration of the desorption process due to convection is evident above certain t_{max} (marked with circles); all data after $t > t_{max}$ were ignored for the fit.